

HYDRODYNAMIC ANALYSIS OF NOISE PROPAGATION BY THE HIGH SKEW MARINE PROPELLER WORKING IN NON-UNIFORM INFLOW

A.HADIPOUR*, K.A.V.ABADI, H.KHANZADI and H.MOTAHARI

Department of Maritime Engineering, Amirkabir University of Technology,
Tehran, IRAN

E-mail: ah160ha99@gmail.com

Being able to predict ship and marine propulsion noise is an important issue for naval architectures and the international maritime community. The main objective of this paper is the numerical investigation on the noise propagation by the high skew marine propeller working in a non-uniform inflow via RANS solver in the broadband frequency range. The pressure fluctuations were monitored at three points on the propeller blade, then by using the FFT operator we computed the blade passing frequency (BPF) for different propeller loading conditions. Based on these pressure pulses and adopting the Fowcs Williams-Hawking model we calculated noise radiated at the monitoring points. The results showed the BPF and noise level increased by increasing the load on the blades and we also observed that the noise generated at the leading edge was greater than at other points. Furthermore, the study of pressure fluctuations showed the propeller tip has more pressure variations in one revolution than other regions of the propeller surface.

Keywords: Noise, high skew marine propeller, pressure fluctuating, blade passing frequency

1. Introduction

The noise produced by marine vessels is important both in intensity and in terms of the spectrum. In recent years, several studies have been focused on understanding and reducing the noise generated by propulsion systems into oceans. Generally, we can divide the source of noise radiated by the marine vessel into four categories [1]:

- noise generated by dynamical devices, main engines, shafting, and gearbox,
- noise caused by cavitation in the propeller,
- acoustic effects associated with variable pressure caused by the propeller,
- flow-induced noise around underwater parts of the vessel hull.

The most significant underwater noise source in a marine vessel is the propeller. Variable pressure on the propeller blade and near the propeller disc induce hull vibration and far-field noise propagation. In commercial vessels, noise generated by the propeller and its effect on the hull are the factors that reduce the comfort of the crew and passengers. Due to the long-term risks of exposure to high-intensity noise within the range of 10 kHz [2], the international maritime organization, IMO, has provided a table including the recommended range of safe noise levels at different locations in commercial vessels [3]. Also, regarding the environment, according to the studies done in recent years to reduce the energy released into the ocean, the propeller noise is one of the undesired issues. One important part of the noise spectrum is the noise that occurs at the blade passing frequency that is equal to the number of blades times the rpm of the rotor.

Generally, any turbulence in the fluid domain caused by the motion or vibration of a solid body such as a rotating propeller in water can be attributed to the production and radiation of acoustic waves. Causes of noise can be generally cavitation and non-cavitation [2]. Reduction and control of pressure oscillation is the

* To whom correspondence should be addressed

most effective way for noise control in marine propellers [4]. An operating propeller in non-uniform inflow caused by the hull and rudder produces strong hydrodynamic pressures fluctuation that generates the undesirable noise. These periodic unsteady hydrodynamic pressure execute separate tonal noise at the blade passing frequency [5] classified with a broadband noise spectrum affected by turbulence interaction with the blade and vortex shedding at the trailing edge and the tips. Accordingly, Tian *et al.* [6] investigated numerically and experimentally the pressure fluctuations at different points on the propeller surface.

On the other hand, the propeller cavitation performance as one of the causes of noise has also been the subject of many studies. Wu *et al.* [7] investigated the noise generated around the high-skew marine propeller in cavitating and non-cavitating conditions with non-uniform inflow. In this study, for the noise prediction the theory of acoustic fan source and the sound radiation theory for spherical bubble were used separately. For cavitating flow the pressure fluctuating in the frequency domain was studied by considering the first blade axial passing frequency. The results of this study showed the intensity of noise propagation by the propeller in cavitating conditions, especially in the range of BPF it was higher than in the non-cavitating condition. Seol *et al.* by coupling the potential-based panel method and time domain acoustic analogy predicted the cavitating and non-cavitating noise generated by the DTMB4119 propeller geometry in non-uniform inflow condition.

In an other study Sakamoto *et al.* [8] used the CFD and semi-experimental formula for predicting cavitation noise. This investigation focused on the four propeller geometry behind the full-scale ship wake. Brown's semi-empirical formula was used for noise estimation in the near field in the upper bound of broadband. This study assumed that hydrodynamic pressure fluctuating is the main source of the cavitation noise. Results show a good agreement of the CFD and Brown's formula. Gorji *et al.* [9] using a RANS solver calculated the sound pressure level around the marine propeller in the low-frequency range. The main factor for the noise generation in this research was pressure pulses and trailing edge vortex. The FWH equation was used for SPL calculation. Results of this numerical study were compared with the experimental data available for the propeller and there was good agreement between these two results.

Ghassemi *et al.* [10] in a numerical investigation calculated the sound pressure level around the marine propeller, DTMB 4382, with different tip rake angles. In this research, two steps of Ffowcs Williams and Hawking equation were used for the pressure and SPL calculation around the propeller via RANS solver. The results showed that increasing the negative or positive rake angle reduces the efficiency and noise propagation by the propeller. In an experimental study, Kowalczyk *et al.* [11] by using the medium-sized cavitation tunnel, studied the noise characteristics generated by a four-blade marine propeller under different loading conditions. A comparison of the results of this method with the numerical method, showed a good agreement between numerical and experimental methods. Park *et al.* [12] used a model test for the estimation of tip vortex cavitation noise and compared the results with novel scaling law that was derived by the Rayleigh-Plesset equation, the Rankine vortex model, the lifting surface theory with physical assumption. As well as the modified ITTC noise estimation rule was also compared with this equation. Results showed that the novel scaling law showed a better agreement than ITTC rules.

An experimentally study by Lee *et al.* [13] used the mass injection for decreasing tip vortex cavitation and noise. A large cavitation tunnel was used for this study. The results of this research proved that water injection is a good technique for reducing tip vortex cavitation and noise. In military vessels, especially submarines, the noise level affects the detection of a vessel and the performance of systems such as sonars [14]. So the design and development of propellers are very important for the optimum level of noise propagation. We can use the hydrodynamic measurement of noise and pressure to identify the potential noise sources on the propeller. There are different methods to predict ship and propulsion system-generated noise such as:

- semi-empirical method,
- potential flow,
- model testing and using a hydrophone,
- hybrid CFD method including FVM software,
- full-scale measurement.

1.1. Mathematical Model

The flow field around the propeller can be predicted by solving the continuity and momentum equations:

$$\frac{\partial \rho}{\partial t} + \frac{\delta}{\delta x_j} (\rho u_i) = 0, \quad (1.1)$$

$$\frac{\partial}{\partial t} (\rho u_i) + \frac{\delta}{\delta x_j} (\rho u_i u_j) = \frac{\delta}{\delta x_j} \tau_{ij} - \frac{\delta p}{\delta x_i} + \rho g_i - \rho \bar{u}_i \bar{u}_j \quad (1.2)$$

where u_i and u_j are velocity components of water, ρ is the density, P is the pressure, τ is the shear stress tensor and $\rho u_i u_j$ is the Reynolds stress tensor. The k - ω turbulent model is the most often used especially for rotating machinery including the marine propeller. In this model, one solves two separate modeled transport equations, one for turbulent kinetic energy and the other for dissipation rate. This equations are as described below:

$$\frac{\partial(k)}{\partial t} + U_j \frac{\partial(k)}{\partial x_j} = P_k - \beta^* k \omega + \frac{\partial}{\partial x_j} \left[(v + \sigma_\omega v_T) \frac{\partial(k)}{\partial x_j} \right], \quad (1.3)$$

$$\frac{\partial(\omega)}{\partial t} + U_j \frac{\partial(\omega)}{\partial x_j} = \alpha s^2 - \beta \omega^2 + \frac{\partial}{\partial x_j} \left[(v + \sigma_\omega v_T) \frac{\partial(\omega)}{\partial x_j} \right] + 2(1 - F_1) \sigma \omega^2 \frac{1}{\omega} \frac{\partial k}{\partial x_j} \frac{\partial \omega}{\partial x_i}. \quad (1.4)$$

The basic equation for the sound propagation was given by Lighthill (1952) [1]. This equation was given

$$\nabla^2 p - \frac{1}{c^2} \ddot{p} = \dot{q} + \nabla \cdot f \frac{\partial^2 \tau_{ij}}{\partial x_i \partial x_j} \quad (1.5)$$

where q expresses the injection of mass or volumetric flow into the fluid. $\nabla \cdot f$ is the divergence of unsteady forces of the fluid. The third component represents the turbulent stress in the fluid. In general, the left side of this equation is related to the sound propagation, and the right side is related to the sound sources. One of the analytic solutions presented for the Lighthill equation is the integral formula to solve it, which was presented by Fox Williams and Hawking (1969) [1]. In FVM software this equation is used for predicting the sound propagation by the propeller. In this method, the flow field solution around the body is identified. This equation is:

$$\begin{aligned} \frac{1}{c_0^2} \frac{\partial^2 p'}{\partial t^2} - \nabla^2 p' &= \frac{\partial^2}{\partial x_i \partial x_j} [T_{ij} H(f)] + \\ &- \frac{\partial}{\partial x_i} \left([P_{ij} n_j + \rho u_i (u_n - v_n)] \delta(f) \right) + \frac{\partial}{\partial t} \left([\rho_0 v_n + \rho (u_n - v_n)] \right) \delta(f) \end{aligned} \quad (1.6)$$

where T_{ij} is the Lighthill stress tensor and it is expressed as

$$T_{ij} = \rho u_i u_j + \delta_{ij} (p - \rho c_0^2) + \tau_{ij} \quad (1.7)$$

where the first term of this equation is the Reynolds stress, the second term is due to changes in pressure and density and the third term is the shear stress tensor. Finally by solving Eq.(1.6) SPL (measured in dB) is calculate by equation (1.8). In this equation, P_{rms} is the root mean square sound pressure and P_{ref} is the reference sound pressure (measured in Pa):

$$SPL = 20 \log_{10} \frac{P_{rms}}{P_{ref}}. \quad (1.8)$$

2. Geometry

In this paper, we used 7 blade high skew marine propeller (Fig.1) and open water hydrodynamic performance data calculated via an experimental test done by Tian et.al [6]. Table.1 shows the specification of the propeller geometry.

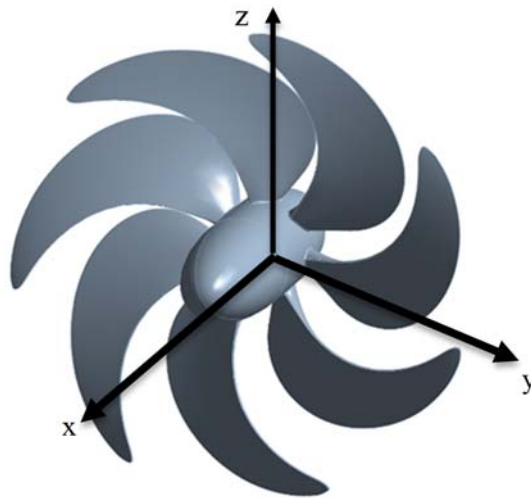


Fig.1. High skew propeller geometry.

Table 1. Geometry specifications.

| Parameter | Value |
|--------------------|-----------|
| Number of blades | 7 |
| Propeller diameter | 0.25 m |
| Expanded area | 0.6 |
| Skew angle | 61 degree |
| Rake angle | 0 |
| Hub ratio | 0.254 |

3. Fluid Domain Modeling

The flow around the propeller is complex because of its geometry so to perform accurate simulation we must use an appropriate computational domain. The cylinder walls have non-slip boundary conditions

(Fig.2 left). The computational domain with the propeller diameter $D = 0.25m$, $24D$ in length, and $16D$ in diameter is shown. For non-uniformizing the flow we used ((+)) bluff body that is shown in Fig.2 (right). For the turbulent model, we used the k-omega SST model and a fluent solver was used for solving this model. The governing equation for this model was solved by the finite volume method based on the RANS equation. In this problem, we used the SIMPLE algorithm for solving the equation of pressure-velocity coupling. Table 2 shows the propeller working condition in 3 states for which we calculated noise propagation. Figure 3 shows the mesh that was generated around the propeller and inflation near the propeller blade.

Table 2. Propeller working conditio.

| State number | Inlet velocity(m/s) | RPM | J |
|--------------|---------------------|-----|------|
| State1 | 1 | 500 | 0.48 |
| State2 | 1 | 600 | 0.4 |
| State3 | 1 | 700 | 0.34 |

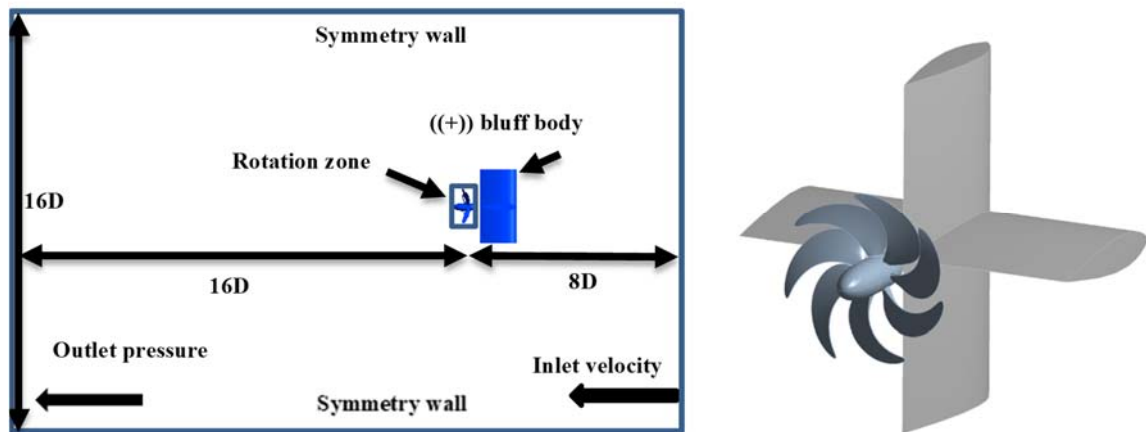


Fig.2. Computational fluid domain (left)propeller with((+)) bluff body ((right)).

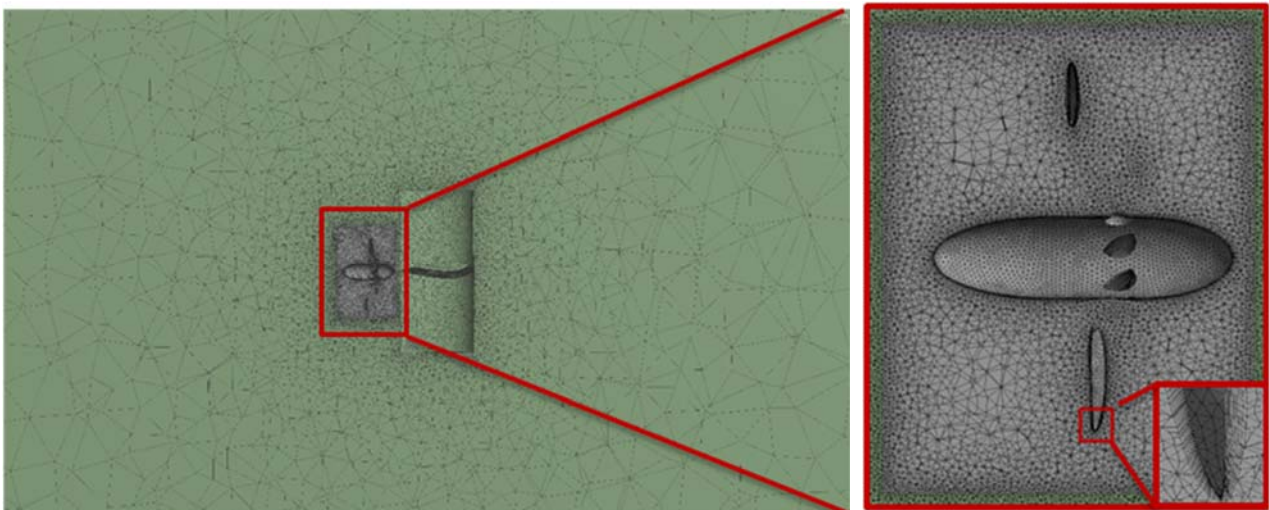


Fig.3. Reduction of the size of the elements near the propeller's blade.

4. Results and discussions

4.1. Open water hydrodynamic performance

The open water characteristics of the propeller can be calculated using non-dimensional coefficients such as the advance coefficient ratio, thrust coefficient, and torque coefficient. This parameter was calculated by using Eqs (5.1). Figure 4 comparez the experimental data that exist in ref. [6] and numerical analysis for this coefficient. As we can see there is a good agreement between the experimental data and numerical analysis

$$K_T = \frac{T}{\rho n^2 D^4}, \quad K_q = \frac{T}{\rho n^2 D^5}, \quad J = \frac{V_A}{nD}, \quad \eta = \frac{JK_T}{2\pi K_q}. \tag{4.1}$$

Table 3. Effect of mesh number on the numerical results.

| Mesh number | Elements | J | K_T (experimental) | K_T (numerical) |
|-------------|-----------|-----|----------------------|-------------------|
| 1 | 10,132,96 | 0.4 | 0.57 | 0.51 |
| 2 | 11,870,47 | 0.4 | 0.57 | 0.53 |
| 3 | 13,275,80 | 0.4 | 0.57 | 0.55 |

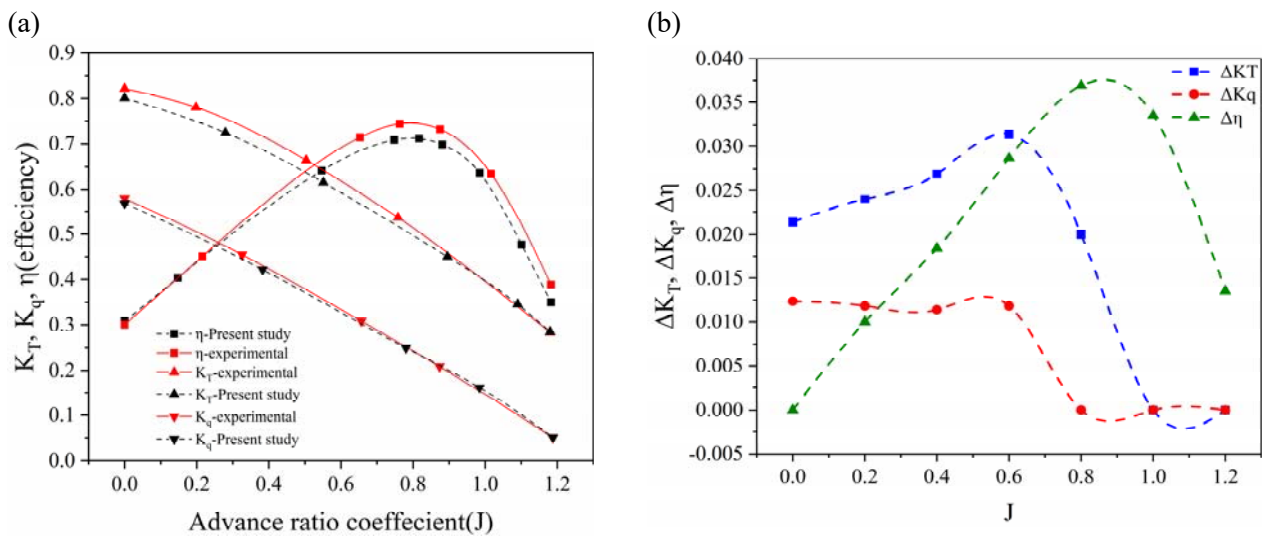


Fig.4. Comparison of computational and experimental hydrodynamic characteristics (a), Relative error in hydrodynamic coefficient (b).

4.2. Pressure fluctuations

Recognition and controlling the pressure fluctuations around the propeller and its surface are some of the ways to study the noise created by the propeller. The pressure fluctuations on the propeller surface, in addition to producing noise, also contribute to the creation of cavitation and induce vibration from the propeller and shaft to the hull. For monitoring the pressure, we will consider 3 points on the blade surface. The first point is on the leading edge of the propeller blade. The leading edge is the first area on the blade that hits the propeller with the fluid flow. The second point is on the propeller tip. Vortex shedding near the tip is one of the most important issues which is caused by a negative pressure pulse and produces a strong noise level in the propeller. The third point is the trailing edge point, causing the negative pulses. Figure 5 shows this three-point on the blade.

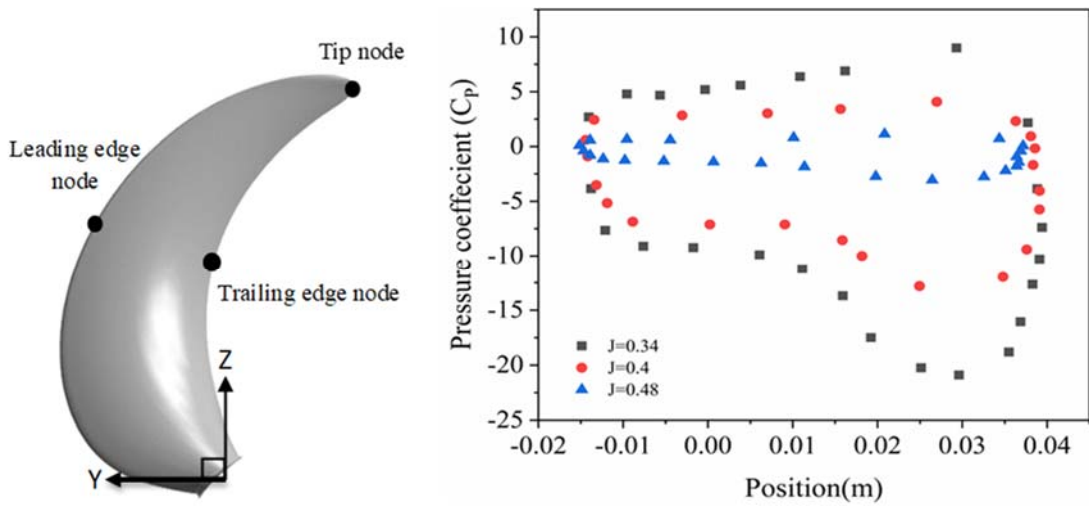


Fig.5. Monitoring node on the blade surface(left) pressure coefficient distribution at $r/R=0.9$ on blade section.

Figure 6 illustrate the inflow velocity and pressure distribution before the propeller. As we can see there are four high velocity and low-pressure regions.

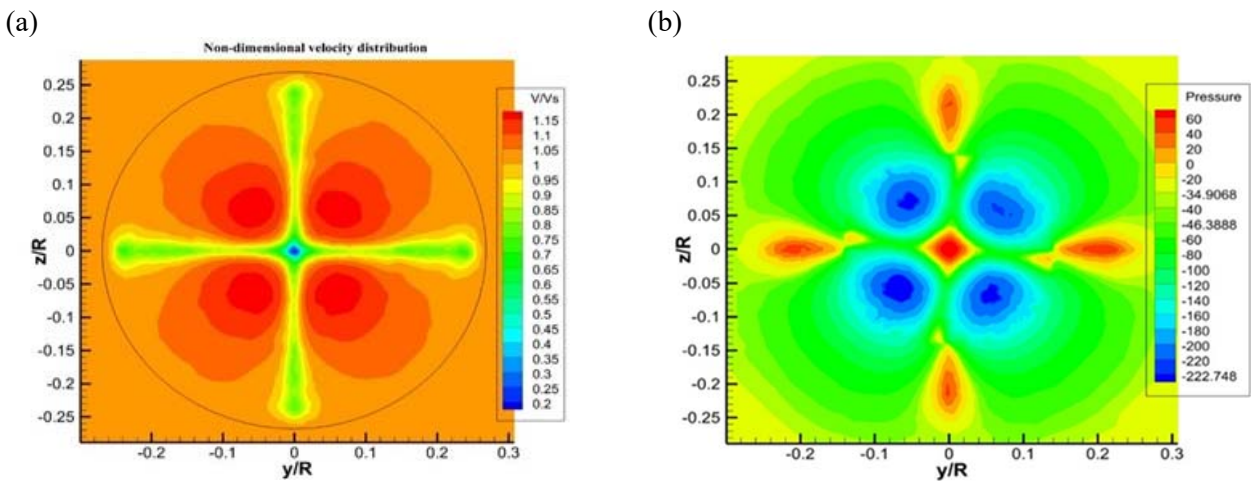


Fig.6. Velocity (a) and pressure distribution (b) before the propeller.

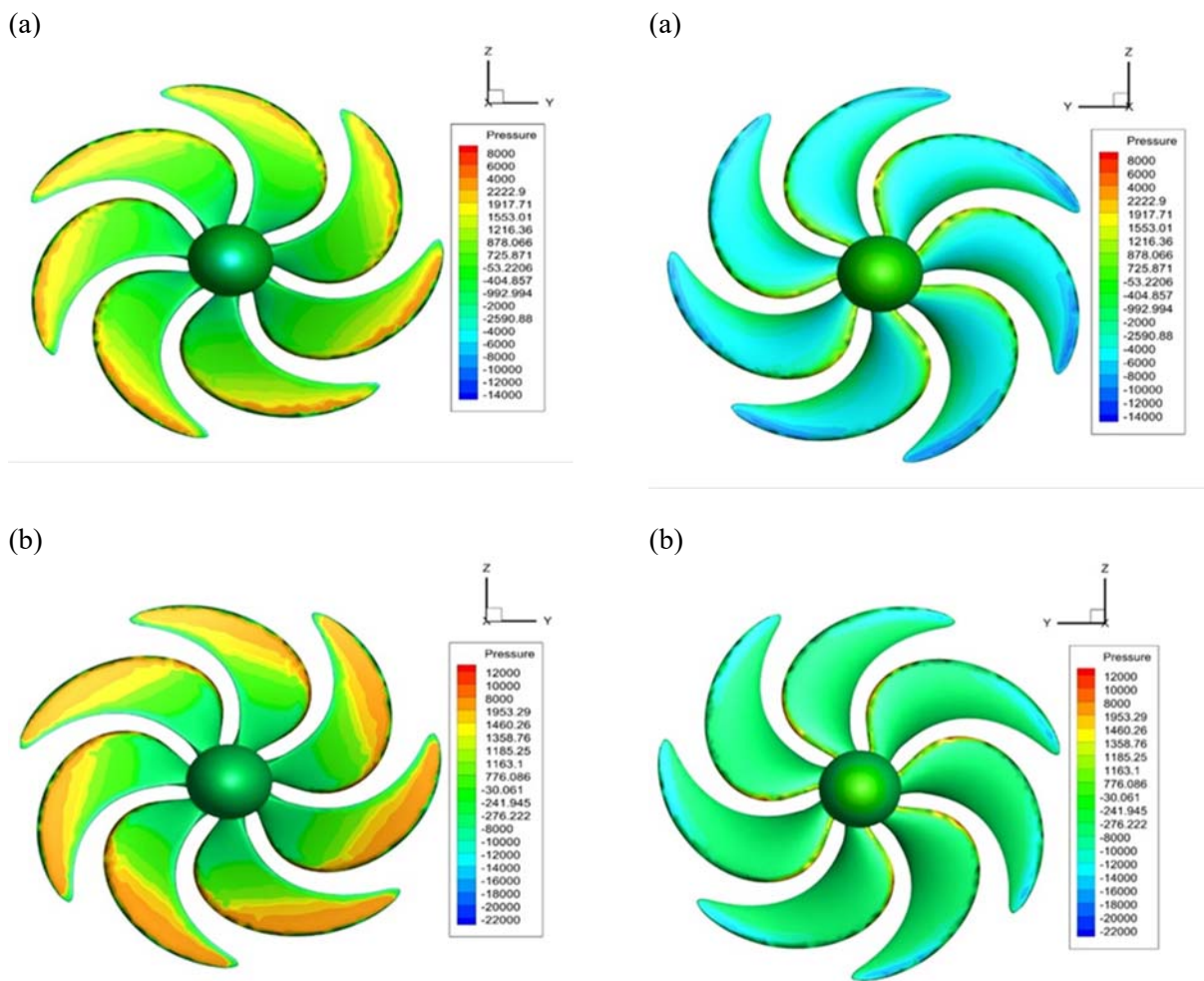


Fig.7. Pressure distribution in pressure side (left column) and suction side (right column) for $J = 0.4$ (a) and $J = 0.34$ (b).

Figure 7 shows the pressure distribution on the suction side and pressure side of the propeller for two loading conditions. We can see in this figure that the pressure distribution near the tip and the leading edge is higher than in other regions. On both sides, the pressure distribution is more intense for $J = 0.34$ than for $J = 0.4$.

Figure 8 shows pressure distribution around the propeller at $J = 0.4$ in six consecutive planes from the center of the propeller. In $x = 0.2R$ we can see negative pressure near the propeller tip that is in the range of $14kPa$. This negative value caused by vortex shedding near the tip and after this negative region there is a positive pressure region bigger than the negative one and finally, we see a range with lower pressure variations before the leading edge. In total, by moving from the tip of the blade to the hub, two regions with negative pressure values are observed, the first which is related to the blade tip and the other related to the trailing edge and hub. These negative pressure regions, in addition to creating sheet cavitation, are important factors in producing near field noise on the blade surface. For $x = 0.6R$, we see a uniform positive pressure range of about $6kPa$. This area is the range impact of the propeller leading region with the fluid domain. Also, we can see for $x = -0.2R$, a low-intensity area marked with pale blue, which is related to the trailing edge and has a negative pressure as the tip of the blade.

In the center of each of the three forms we can see that, the negative pressure region created around the hub is intense, which can also be attributed to the Hub Vertex phenomenon. For $x = 0.6r$, we see low-pressure variation greater than in the other planes.

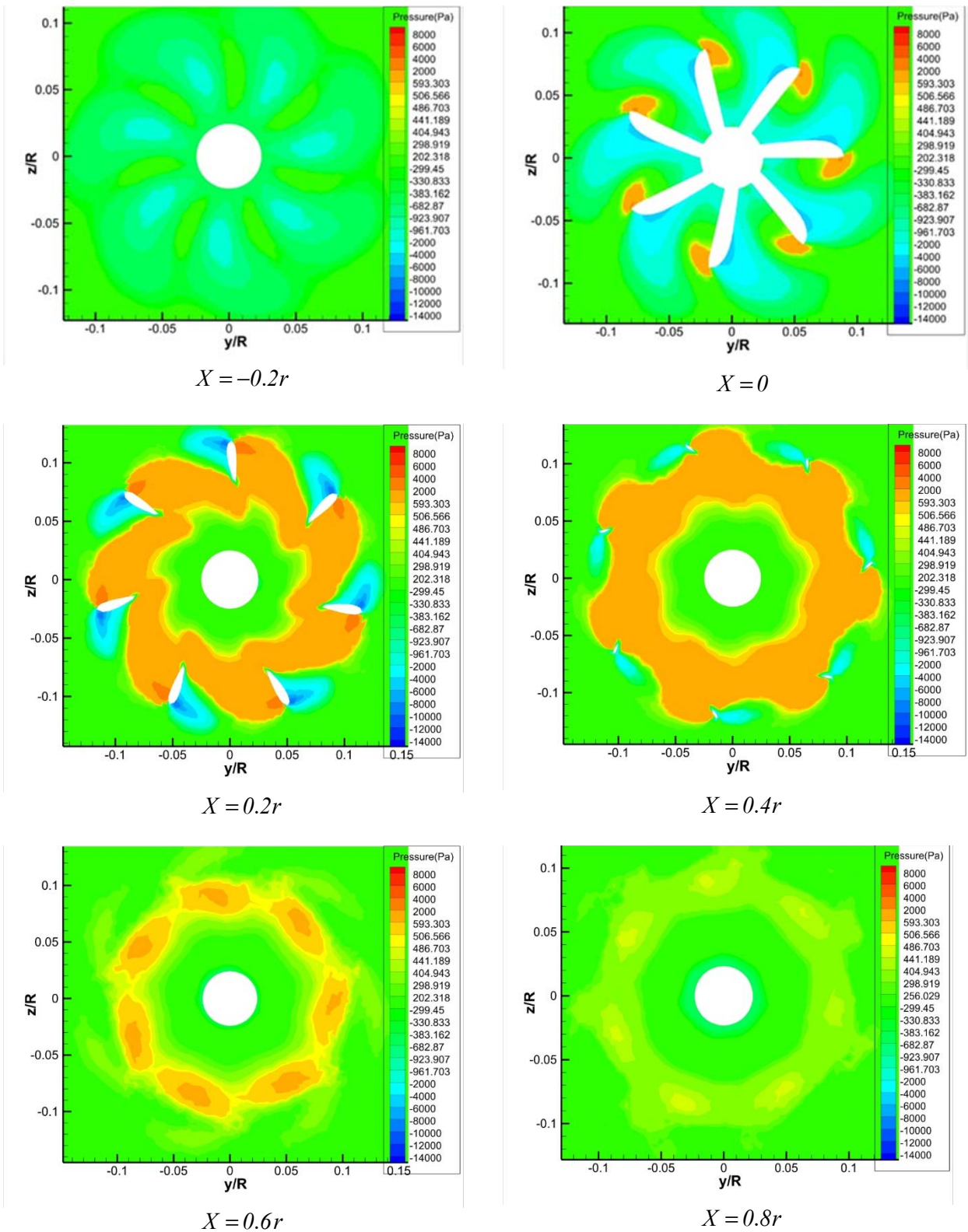


Fig.8. Pressure distribution around the propeller for $J = 0.4$.

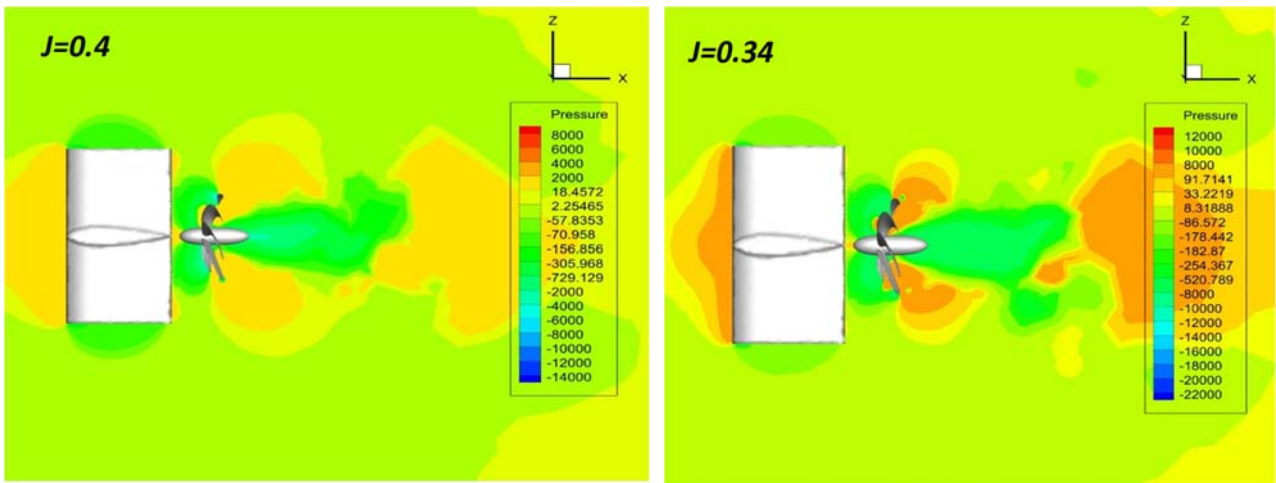


Fig.9. Pressure distribution in downstream for two working condition.

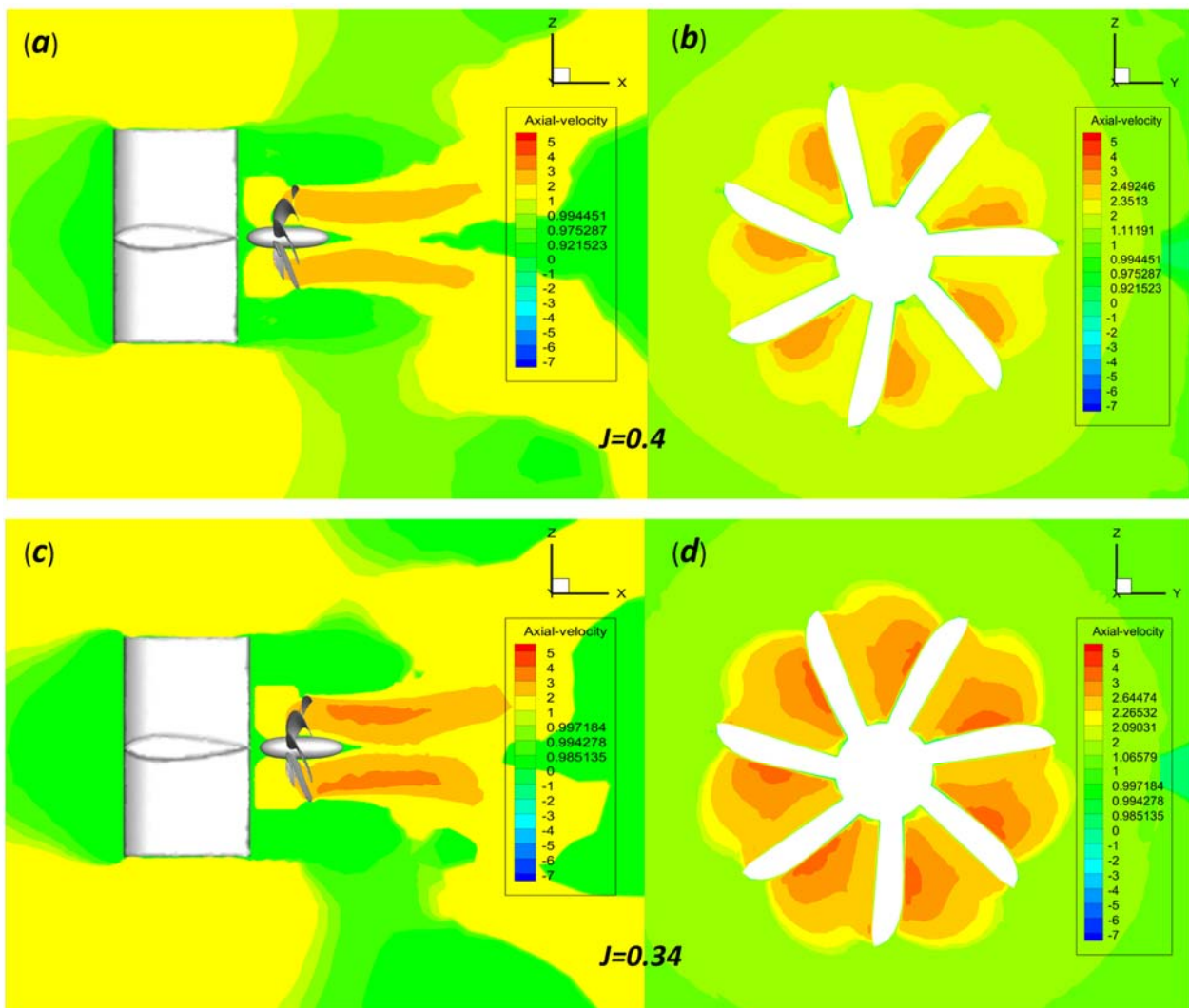


Fig.10. Axial velocity distribution in blade section (right) and downstream (left).

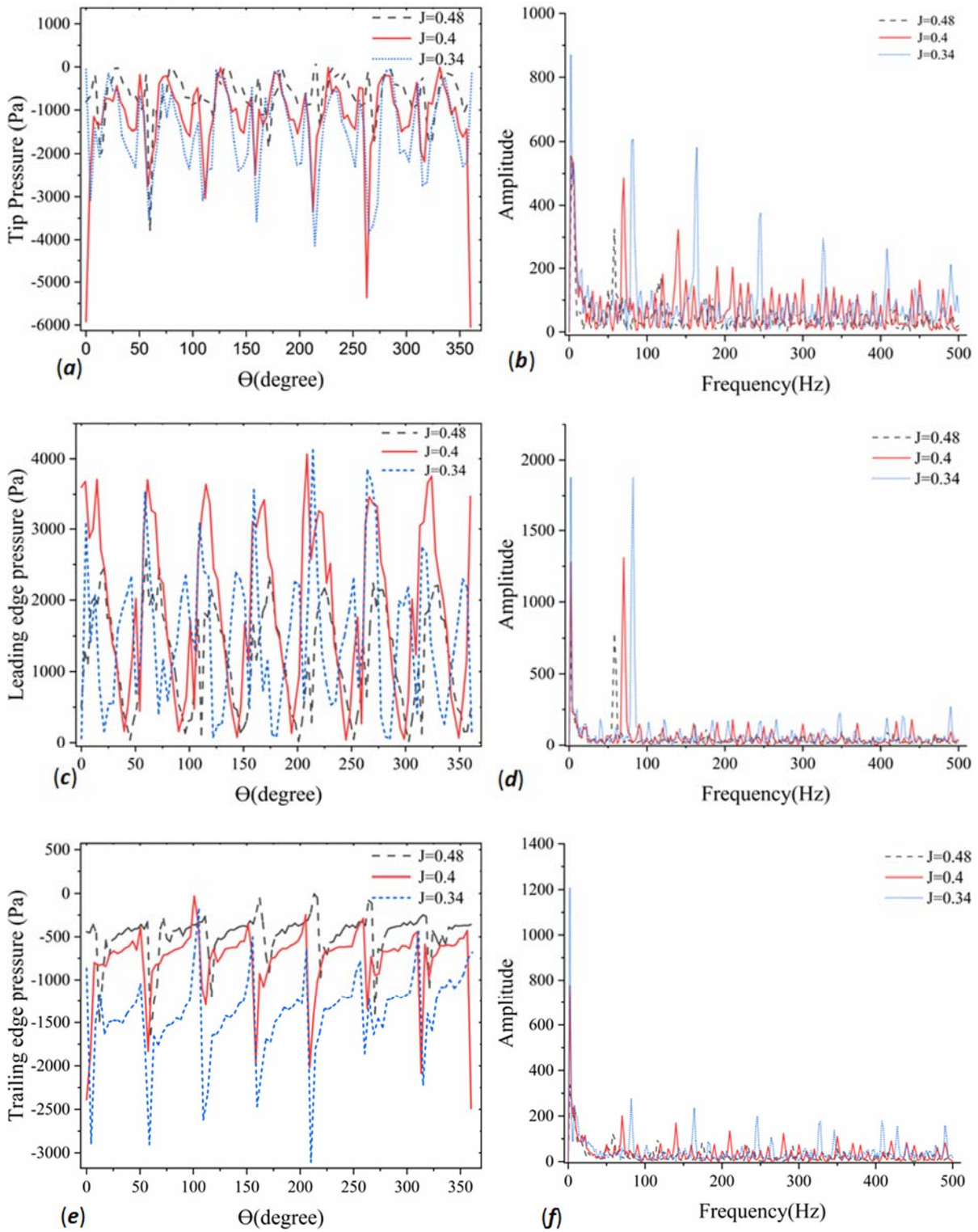


Fig.11. Pressure fluctuations in 1 revolutions for 3 location on the propeller blade (left column) and fluctuations in the frequency domain (right column).

Figure 9 shows the pressure distribution for two working conditions in downstream. As we can see maximum pressure is created near the propeller tip and minimum pressure is created near the hub and root of

the propeller. Also, it can be seen that the intensity of the pressure distribution in downstream for $J = 0.34$ is higher than for other working conditions.

Figure 10 illustrates the axial velocity distribution in the blade section and downstream for $J = 0.4$ (a, b) and $J = 0.34$ (e, d). In this figure, we can observe the high-velocity region in the blade section near the trailing edge and near the tip at the downstream. Also, the difference in velocity between the pressure side and the suction side of the propeller can be observed as the main reason for the thrust generation.

It should be noted that the pressure values recorded at the locations described are related to the area around the blade. The pressure fluctuations on the blade surface, are presented in Fig.11. It shows pressure fluctuations registered in one revolution of the propeller. As we can see in Fig.11. (a) the pressure fluctuations for the propeller's tip-in three working conditions are computed. In this graph, the maximum value of pressure occurred at $J = 0.4$ but the highest number of oscillations is at $J = 0.34$. For the leading edge pressure oscillations (Fig.11 (c)) pressure values for most of the peaks occurring for both working conditions 2 and 3 are approximately the same, but the number of fluctuations in 2 is the same as in the previous case. Figure 11 (e) shows pressure oscillations at the trailing edge and as we can see, $J = 0.34$ has a maximum value of pressure and oscillations.

By observing the oscillations in the frequency domain shown in Fig.11 (b, d, f) it can be seen that the first peak is for all three modes in the range of 2 Hz and then for $J = 0.48$ at 50 Hz , $J = 0.4$ at 72 Hz , and in $J = 0.34$; 82 Hz . This result is in good agreement with the study made by Tian [6], which calculated the Blade Passing Frequency of 70 Hz .

5.3. Noise Analysis

The noise produced on the propeller blade includes periodic pulses, which are divided into separate ranges by passing the frequency of BPF (Blade Passing Frequency). The most important part of this frequency range is in the area of broadband caused by the vortex shedding and turbulent inflow at the tip and trailing edge [10].

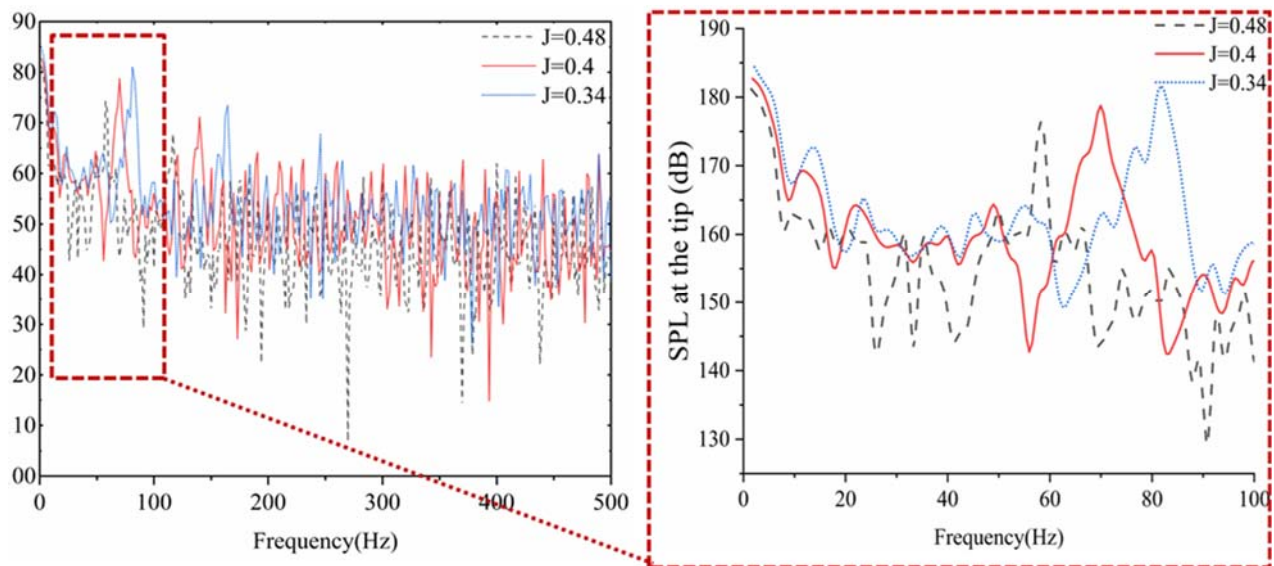


Fig.12. Sound pressure level at the tip.

Generally, the noise that is used to detect and identify marine vessels can be classified into three categories [15]:

- thrust noise, in the low-frequency range ($< 100\text{ Hz}$);

- tip and Trailing edge noise ($200 - 1000 \text{ Hz}$);
- broadband noise ($100 - 1000 \text{ Hz}$).

On the other hand interaction of the turbulent inflow and the leading edge is another source of noise in the broadband range. Based on the numerical results of the pressure fluctuating we calculate the SPL for 3 specified points on the blade. Figure 12 shows the spectrum analysis of the sound pressure level at the tip in three working conditions. This graph shows the maximum level of noise that happened at the blade passing frequency for each working condition. For example, at $J=0.4$ BPF occur at 72 Hz and SPL for this frequency is 177 dB . It has also been seen by comparing the two working conditions $J=0.4$ and $J=0.34$. $J=0.34$ is a heavier working condition and the noise level is also higher. Considering the importance of producing noise in the BPF range with a magnification of noise at a frequency of $(0 - 100) \text{ Hz}$ for each of the three points studied, we will study the noise radiation in this range more precisely.

As we can see, the maximum noise level is initially at a frequency of 2.4 Hz . Generally, it can be seen that noise fluctuations are less than the frequency range of $(100 - 500) \text{ Hz}$.

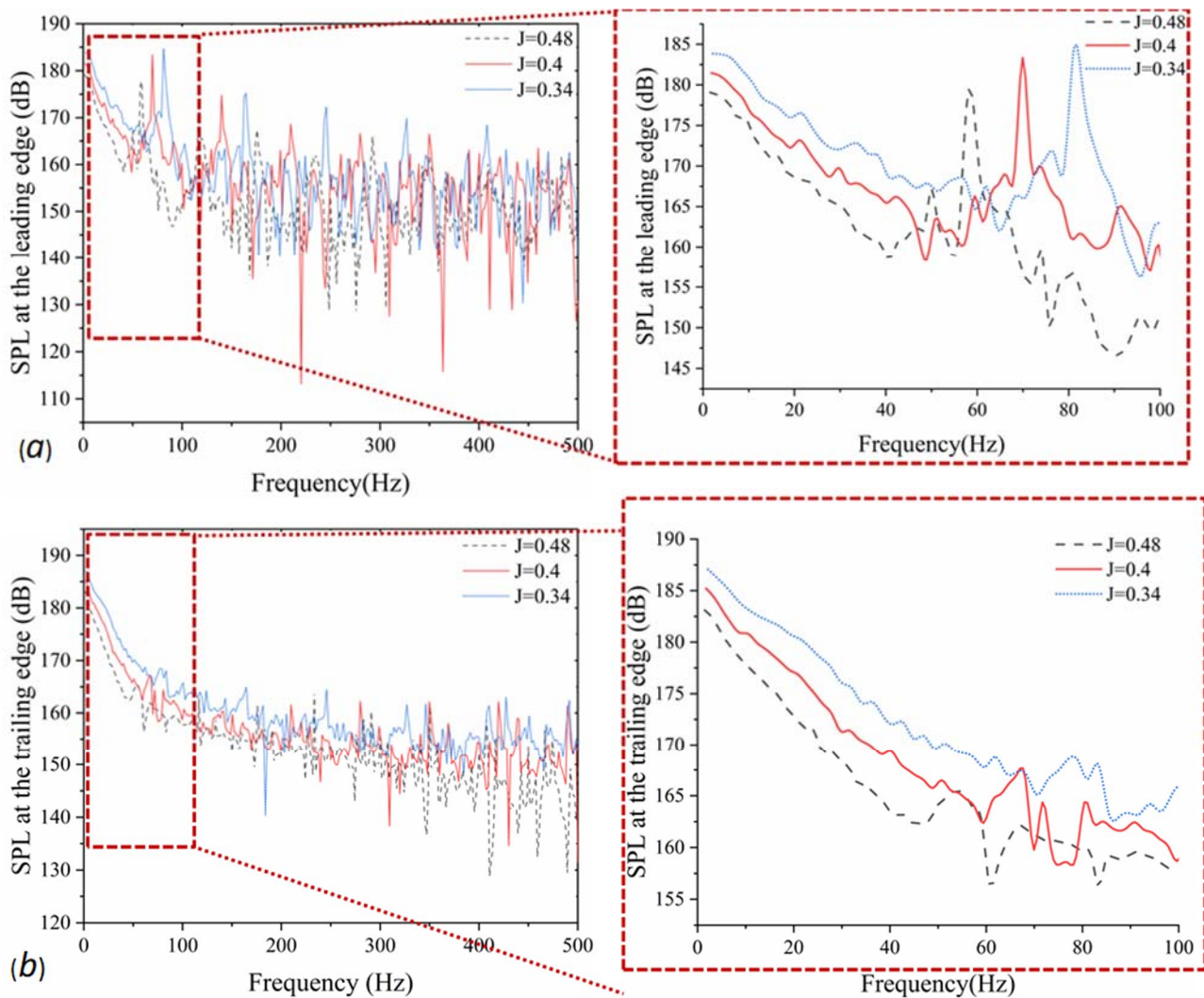


Fig.13. Sound pressure level at the leading edge point (a) and trailing edge point (b).

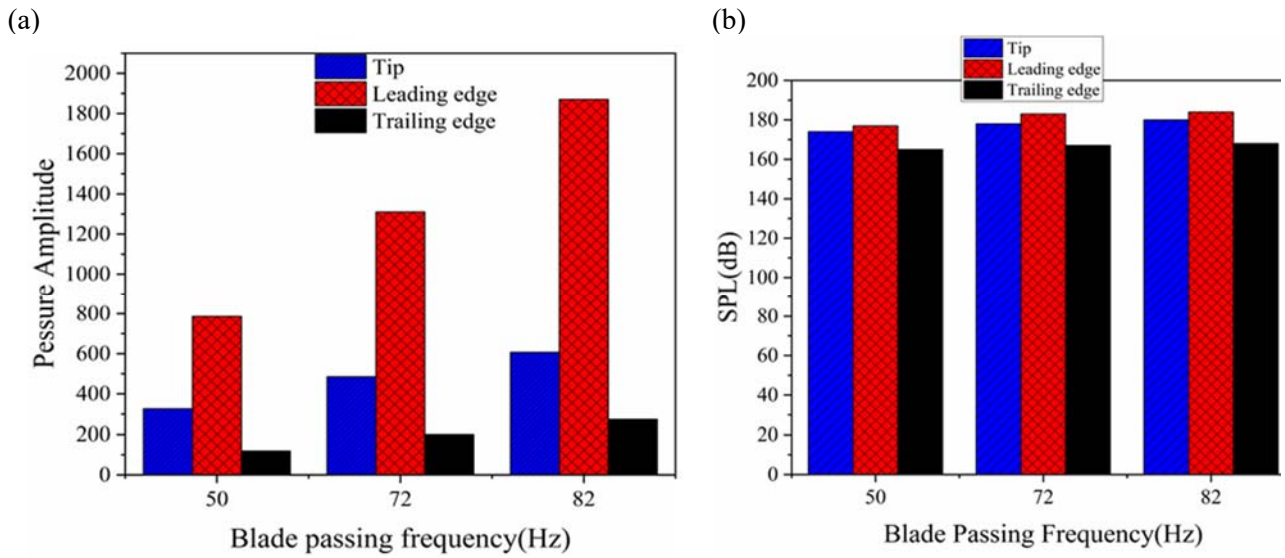


Fig.14. Comparison of pressure amplitude in BPF(a) and comparison of SPL in BPF(b).

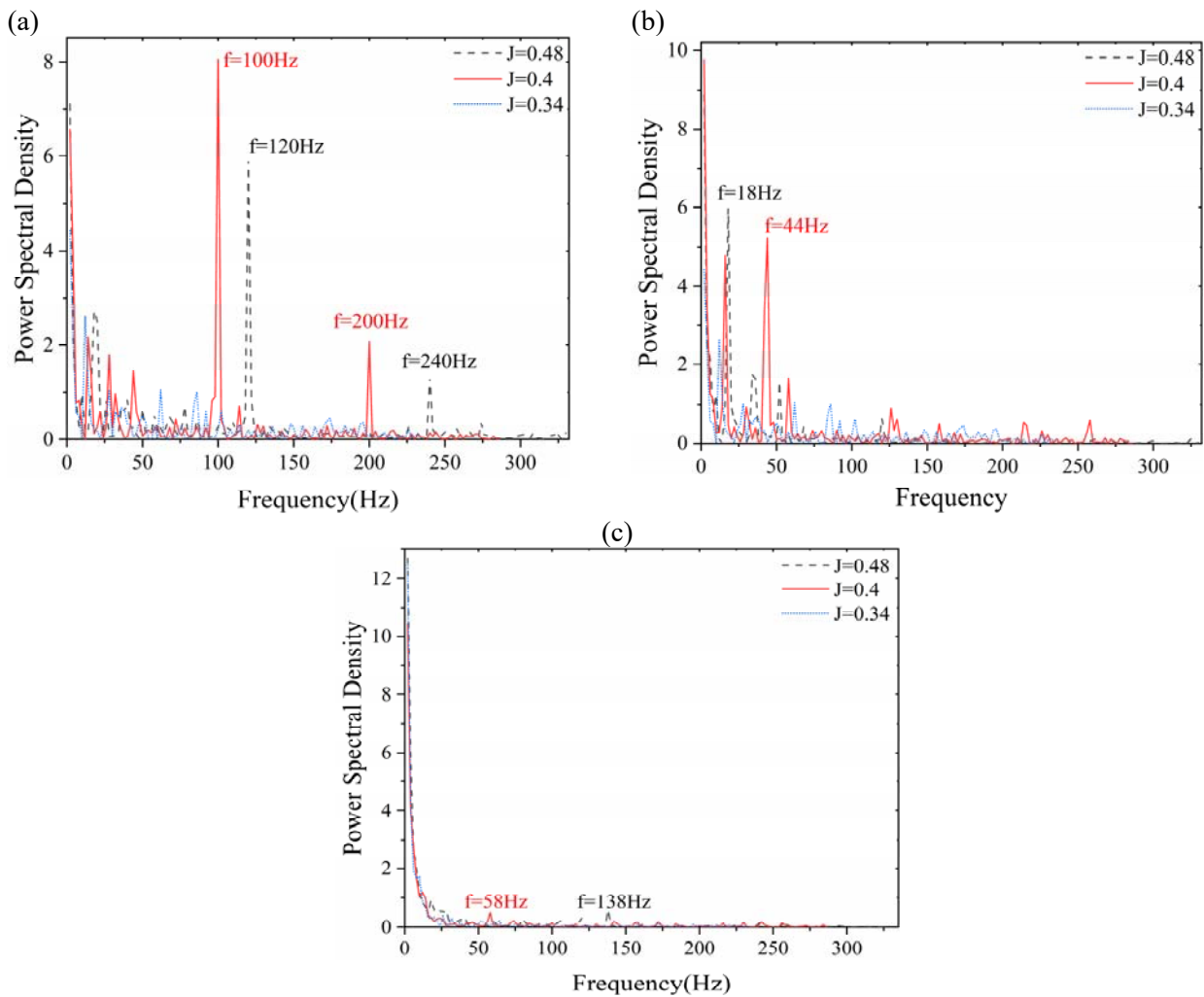


Fig.15. Power spectral density of the tip (a), leading-edge (b) and trailing edge (c).

Figure 13(a) shows the sound pressure level on the leading edge. Also Fig.10 (b) shows the SPL at the trailing edge point. Similarly, by zooming in the frequency range at the beginning of the chart we can study noise propagation at BPF better.

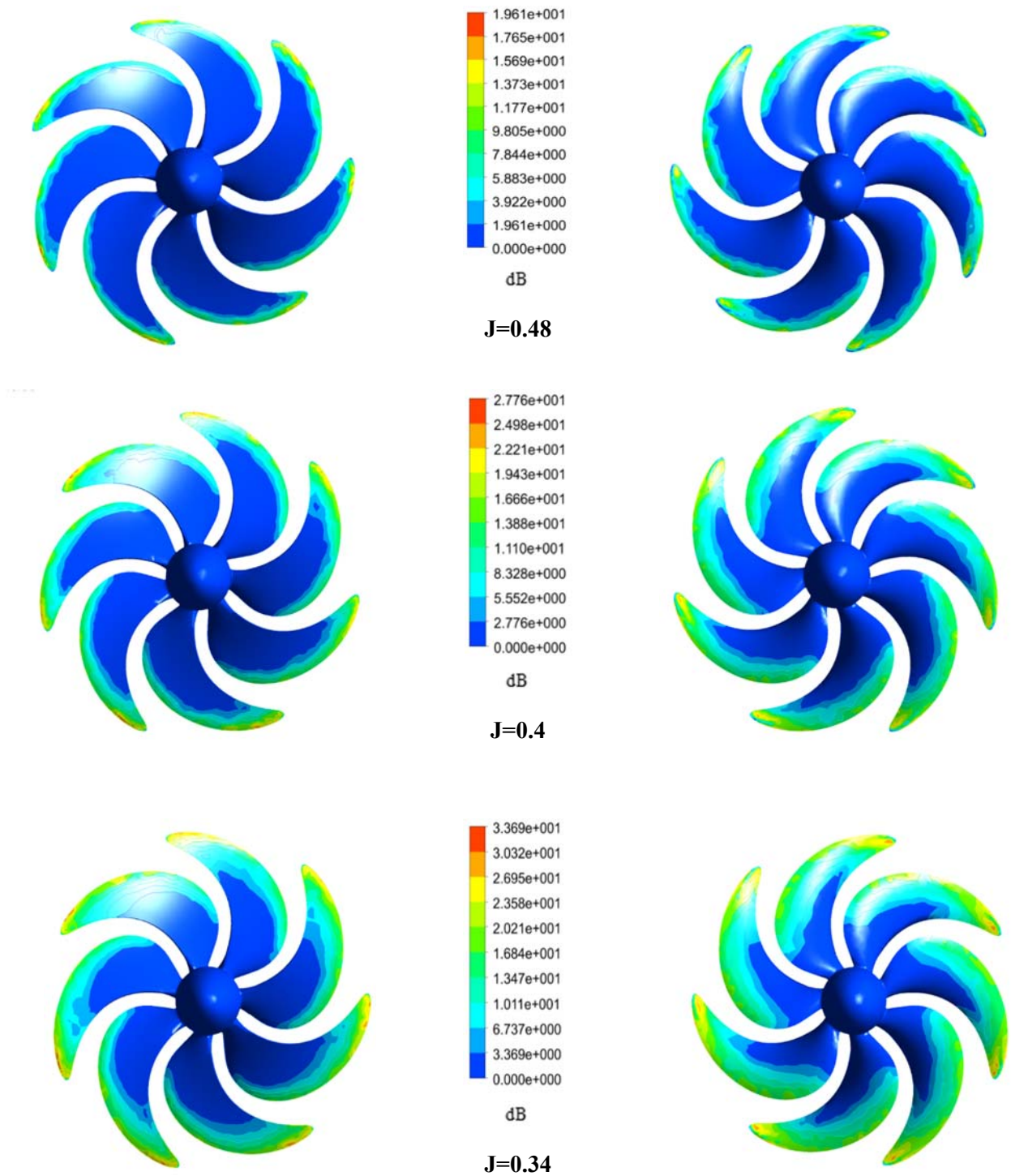


Fig.16. SPL distributions for 3 loading condition in the suction side (right column) and pressure side (left column) of the propeller surface.

The noise power spectrum (NPS) analysis is a useful image quality metric that provides a measurable description of the amount and frequency of noise [15]. This is illustrated in Figure 11.

Figure 14(a,b) shows a comparison of the pressure amplitude and SPL at the three different working conditions and their relative BPFs.

Figure 15 illustrated the power spectral density analysis of tip and leading-edge noise based on the noise fluctuations. As we can see in Fig.11(a) there are five peaks of acoustic energy and the maximum energy can be seen at 100Hz that is associated with $J=0.4$ also the amount of this energy for $J=0.48$ greater than $J=0.34$ and the largest value of acoustic energy at the tip is 8 . Figure 11(b) shows noise energy for the leading edge. The maximum value of energy occurs around 18Hz frequency order and its related to $J=0.48$ but this peak after the biggest peak at the beginning of the chart and the maximum number of density peak for the $J=0.4$ that is five. Figure 15(c) shows noise energy for the trailing edge. As we can see, the noise generated by the trailing edge has less intensity than the other two nodes. For all three working conditions at the beginning of the chart, there is a peak at 4 Hz frequency that has a higher amplitude. After that, two other peaks are seen at frequencies of 58 and 138 Hz , with very mild intensity.

Figure 16 shows the SPL distribution on the propeller surface. As shown in this figure, SPL intensity on propeller blades increases by increasing the loading condition.

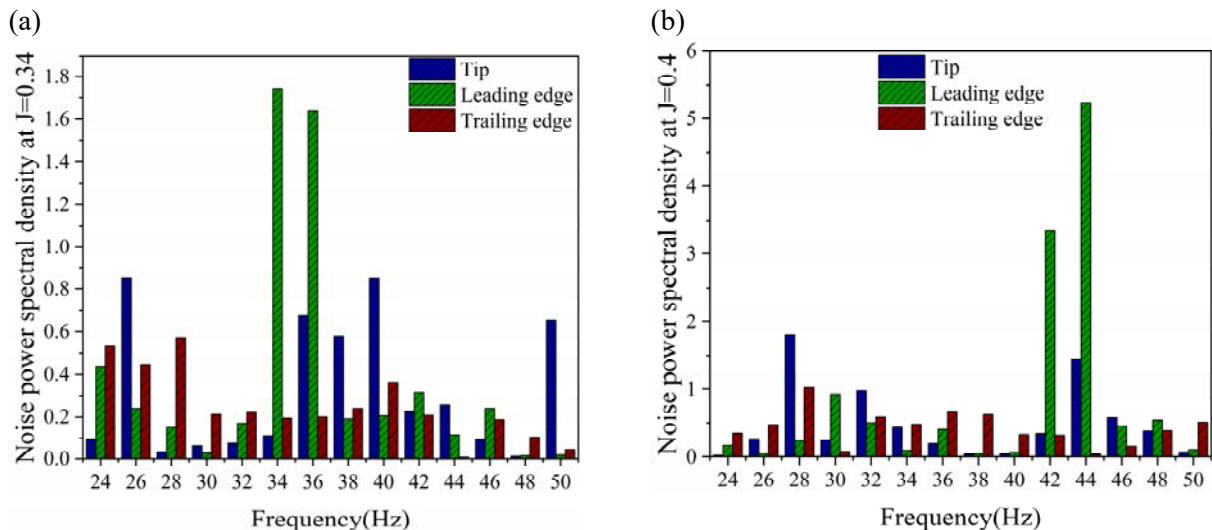


Fig.17. Comparison of noise power spectral density at $J=0.34$ (a) and $J=0.4$ (b).

Figure 17 shows the noise power spectral density comparison between two working conditions $J=0.4$ and $J=0.34$. As can be seen in this figure, the maximum noise level for the frequency range specified in the frequencies 34 and 36 Hz for mode 1 and 42 and 44 Hz frequencies for mode 2 occurred.

6. Conclusion

The main objective of this study was to numerically investigate the noise propagation by pressure pulses with 7 blade high skew marine propeller. At first, three different working conditions were defined for the propeller, and then we studied the pressure distribution on the propeller surface and its nearfield. The values of pressure fluctuations were calculated and compared for the three-nodes marked on the blade. Then based on pressure monitoring and based on Fowcs William-Hawking we calculated sound pressure level (SPL) and power spectral density of SPL. The primary finding include:

- 1) Pressure fluctuations in the tip of the blade are higher than at the other two points in terms of amplitude and intensity. This can be seen by studying fluctuations in the frequency domain.

- 2) By increasing the loading on the propeller, the intensity of pressure fluctuations is significantly increased, as shown in Fig.11(a, c, e).
- 3) By increasing the loading on the propeller the blade passing frequency will also increased. It's also at $J = 0.34$ equal to 72 Hz , which is in good agreement with the study by Tian.
- 4) The oscillation of noise released at the leading edge of the propeller is greater than at the other two points, and its intensity in $J = 0.34$ is also greater in the other two working conditions.
- 5) The highest amount of noise has occurred for all three points in the BPF range.
- 6) The lowest amount of noise energy was produced at the trailing edge. It also has a maximum value at frequencies of $4, 100,$ and 120 Hz at the tip and frequencies of 4 and 18 Hz at the leading edge.

Nomenclature

| | |
|------------|---|
| D | – diameter |
| P | – pressure |
| $pu_i u_j$ | – the Reynolds stress tensor |
| P_{rms} | – the root mean square sound pressure |
| P_{ref} | – reference sound pressure |
| q | – the injection of mass or volumetric flow into the fluid |
| T_{ij} | – the Lighthill stress tensor |
| u_i, u_j | – velocity components of water |
| ρ | – density |
| τ | – the shear stress tensor |

Reference

- [1] Bjørnø, L. (2017): *Underwater Acoustic Measurements and Their Applications*.– In Applied Underwater Acoustics, Elsevier, pp. 889-947.
- [2] Carlton, J., 2019: *Marine Propellers and Propulsion*.– Butterworth-Heinemann, 4th edition, p.586.
- [3] IMO (1981): *Code on Noise Levels on Board Ships*.– International Maritime Organization, p.16.
- [4] Chekab M.A.F., Ghadimi P., Djeddi S.R. and Soroushan M. (2013): *Investigation of different methods of noise reduction for submerged marine propellers and their classification*.– American Journal of Mechanical Engineering, vol.1, No.2, pp.34-42.
- [5] Madsen H.A. (2010): *Low frequency noise from wind turbines mechanisms of generation and its modeling*.– Journal of Low Frequency Noise, Vibration and Active Control, vol.29, No.4, pp.239-251.
- [6] Tian J., Yang H., Zhang Z. and Yuan G. (2014): *LES-based numerical analysis of surface-pressure fluctuations and unsteady thrust of a marine propeller*.– In INTER-NOISE and NOISE-CON Congress and Conference Proceedings, vol.249, No.8, pp.441-448.
- [7] Wu Q., Huang B., Wang G., Cao S. and Zhu M. (2018): *Numerical modeling of unsteady cavitation and induced noise around a marine propeller*.– Ocean Engineering, vol.160, pp.143-155.
- [8] Sakamoto N. and Kamiirisa H. (2018): *Prediction of near field propeller cavitation noise by viscous CFD with a semi-empirical approach and its validation in the model and full scale*.– Ocean Engineering, vol.168, pp.41-59.
- [9] Gorji M., Ghassemi H. and Mohammadi J. (2018): *Calculation of sound pressure level of marine propeller in low frequency*.– Journal of Low Frequency Noise, Vibration and Active Control, vol.37, No.1, pp.60-73.
- [10] Ghassemi H., Gorji M. and Mohammadi J. (2018): *Effect of tip rake angle on the hydrodynamic characteristics and sound pressure level around the marine propeller*.– Ships and Offshore Structures, vol.13, No.7, pp.1-10.
- [11] Kowalczyk S. and Felicjancik J. (2016): *Numerical and experimental propeller noise investigations*.– Ocean Engineering, vol.120, pp.108-115.

- [12] Park J., and Seong W. (2017): *Novel scaling law for estimating propeller tip vortex cavitation noise from the model experiment.*– Journal of Hydrodynamics, vol.29, No.6, pp. 962-971.
- [13] Lee C.S., Ahn B.K., Han J.M. and Kim J.H. (2018): *Propeller tip vortex cavitation control and induced noise suppression by water injection.*– Journal of Marine Science and Technology, vol.23, No.3, pp.453-463.
- [14] Andersen P., Kappel J.J. and Spangenberg E. (2009): *Aspects of propeller developments for a submarine. In First international symposium on marine propulsors.*– Conference: The First International Symposium on Marine Propulsors: SMP'09, Trondheim, Norwegian Marine Technology Research Institute (MARINTEK), pp.551-561.
- [15] Cupp S.L. (2008): *A practical application for noise power spectrum analysis (MSc Thesis).*– Drexel University, p.79.

Received: September 21, 2019

Revised: November 9, 2020